



Full Length Article

Cleat structure analysis and permeability simulation of coal samples based on micro-computed tomography (micro-CT) and scan electron microscopy (SEM) technology

Alexandra Roslin, Dubravka Pokrajac, Yingfang Zhou*

School of Engineering, University of Aberdeen, Aberdeen AB243UE, United Kingdom

ARTICLE INFO

Keywords:

Coal bed methane
Micro-CT
SEM
Subvoxel algorithm
Permeability
Lattice Boltzmann method

ABSTRACT

Coal has been playing an important role as a valuable source of energy for many years. In turn, gas production from coal reservoirs is a modern development and coal bed methane (CBM), also known as coal seam gas (CSG), is attracting global attention due to its wide occurrence and benefits for the environment as opposed to the conventional energy sources. Developing coal bed methane reservoirs requires better understanding of the flow behaviours of gas and liquids in cleats and analysis of possible contribution of pores to the flow. This paper describes the implementation of micro computed tomography (micro-CT) and scan electron microscopy (SEM) techniques for analysis of coal samples. Intermediate rank coal samples used in this study were collected from Southern Qinshui Basin (China). In the course of the described research, coal samples were scanned, processed and segmented to study the cleat spacing and permeability. Due to the partial volume effect, the resolution of cleats needed improvement which was achieved by subvoxel processing using a novel algorithm as explained in detail in the paper. Permeability was obtained through simulation of one phase flow using Lattice Boltzmann method (LBM). The results show that the simulated permeability is comparable to the analytical approximation. The subvoxel processing has proved an effective method of overcoming the partial volume effect for the low resolution micro-CT images.

1. Introduction

Coal seam gas (CSG), also known as coal bed methane (CBM), is a form of unconventional natural gas extracted from coal reservoirs. Unconventional resources are those hydrocarbon reservoirs whose permeability/viscosity ratio requires use of technology to alter either the rock permeability or the fluid viscosity, or both, in order to produce them at commercially competitive rates. Unlike conventional clastic deposits, coal seams contain a high proportion of mostly localised organic matters in addition to inorganic material. This results in dual-pore system where pores in organic matter are often too small to be efficient flow paths, whereas much larger fractures (known as cleats) are believed to be main conducts from which gas in organic matters can flow out [6,25,29]. Develop coal bed methane reservoirs demands better understanding of the flow behaviour of gases and liquids in pores and fractures. This may require the use of sub-micron resolution data for calculation of reservoir petrophysical properties and simulation of gas/water flow behaviour. In turn, the latter demands thorough comprehension of the pore space structure of rocks. Micro-computed

tomography and scanning electron microscopy provide an effective source of information on the internal structure of coal porous space.

The evolution of modern micro-CT imaging techniques is based on three-dimensional reconstructions from a series of two-dimensional projections taken at different angles: the sample is rotated and the absorption of X-rays in different directions is recorded and used to produce a three-dimensional representation of the rocks and fluids [3]. The main advantage of X-ray micro-computed tomography is that it yields high-resolution three-dimensional images of solid opaque objects quickly and non-destructively [5]. It is similar to medical CT scanning, but carried out on a smaller scale and with greatly increased resolution (down to less than 1 μm is possible) [11]. Implementation of such imaging is of value in a variety of applications, including examination of clastic [10,19], fractured basement [20] and carbonate [1] reservoir rocks, as well as three-dimensional studies of coal [24], paper [31], biomaterials [18], bones [41], volcanic ash [7], materials for palaeontology [23], soil science, meteorites, and geotechnics [17].

In synchrotrons, which were exploited for first micro-CT images of rocks, a bright monochromatic beam of X-ray is shone through a small

* Corresponding author.

E-mail address: yingfang.zhou@abdn.ac.uk (Y. Zhou).

rock sample [8]. The now-standard approach for scanning the pore space of rocks is to use a laboratory instrument, a micro-CT scanner, which houses its own source of X-rays [2]. The X-rays are polychromatic, and the beam is not collimated – the image resolution is determined primarily by the proximity of the rock samples to the source [3]. The intensity recorded for the pixels (2D) and results from reconstruction for the voxels (3D) obtained in micro-CT analysis represents the relative radio density, or relative attenuation of X-rays through individual segments of the imaged material [27]. Within the tomogram, the X-ray opacity of the material in each individual segment determines its brightness, allowing a three-dimensional image to be reconstructed from sections viewed at different angles [11]. Voids are usually represented as black in micro-CT images due to their low X-ray opacity, minerals are usually light grey (or white) to medium grey due to intermediate X-ray opacity [11].

Many researchers have exploited computed tomography for quantitative characterisation of fractures in coal (e.g. [24,35] etc.). Other researchers used micro-CT techniques to investigate gas adsorption and desorption in coal (e.g. [15], as well as to investigate the heterogeneity and spatial distribution of pores [9], fractures [40] and distribution of organic and mineral matter (e.g. [36,34] in coals of different rank. The behaviour of fluids in pore space of rocks was extensively examined, but those research studies mostly concentrated on sandstones (Berea sandstone etc.) and carbonates (for example, Estailades carbonate) [3], with only a few focusing on simulation of gas flow in porous space of coal (e.g. [14].

In addition to 3D imaging methods, there are other methods, well established in two dimensions, for producing very fine images of rock samples. Amongst them the most widely applied is SEM (scanning electron microscopy) which produces images down to resolution of 10 s nm [3]. SEM is a technology which generates ultra-high resolution two-dimensional images of thin rock samples [21]). As opposed to micro-CT, this method is destructive, but its advantage is that it allows revealing details of small pores which are beyond the resolution of micro-CT images. SEM images are often used to: provide details which are beyond the resolution of micro-CT images [11,30]; calibrate micro-CT images [26]; generate synthetic 3D structures from two dimensional thin sections[39].

For the purpose of the research described in this paper, micro-CT techniques were used in conjunction with electron microscopy to obtain sufficiently detailed images of intermediate rank coal sample and to segment the cleats of those images. The studied samples are characterised by irregular cleat system which contains mainly thin, poorly resolved fractures due to the partial volume effect. The subvoxel processing algorithm was applied in order to overcome that effect and to improve the quality of the images. The subvoxelled images were then segmented and used for simulating of single-phase flow through the pore space of coal samples. The idea of the subvoxel algorithm was taken from the medical study of trabecular bones [13] but the algorithm was written for coal and it has never previously been used for rock sample micro-CT images. The study described in this paper concentrated on mm-scale effects. Upscaling of these results to the larger scales was the objective of a follow-up study.

2. Samples and samples preparation

Samples of intermediate rank coal from Panlong mine in Southern Qinshui coal bed methane basin (China) were obtained and examined, the samples are buried in a range of 600–750 m subsurface and in this work one sample (Fig. 1) was chosen in order to analyse cleat porosity and permeability.

The main characteristics of the analysed coal sample acquired from coal proximate analysis are listed in Table 1.

Previous studies (e.g. [37,4] show that the coal from this basin contain 0.59–3.54% moisture, 3.5–15.54% ash yield, 73.62–88.92% fixed carbon and 2.14–4.04% hydrogen, with C/H ratios in the range of



Fig. 1. Coal core sample in a sample holder used in this study.

19.96–36.25. The vitrinite reflectance ranges from 1.95 to 3.49%, with 18.5–97.4% vitrinite and 2.4–81.4% inertinite. The gas in-place concentration is in the range from 0.72 to $2.88 \times 10^8 \text{ m}^3/\text{km}^2$, with an average of $1.21 \times 10^8 \text{ m}^3/\text{km}^2$.

Samples were not dried or saturated with any high contrast fluid to preserve samples integrity. For SEM analysis, the sample surface was polished in three different directions and carbon-coated (see Fig. 2).

3. Methodology

X-ray micro-computed tomography was conducted using the laboratory-based ZEISS VersaXRM-410 3D microscope (Fig. 3), which delivers non-destructive 3D imaging with submicron resolution, for in situ scanning, and provides high-resolution micro-CT images for the widest range of sample sizes. This machine uses patented detectors which convert X-rays into visible light and then uses a microscope turret of objectives for easy and accurate zooming. VersaXRM-410 achieves $0.9 \mu\text{m}$ true spatial resolution with minimum achievable voxel size of 100 nm. Advanced absorption and phase contrast (for soft or low-Z materials) provide greater versatility in overcoming the limitations of traditional computed tomography (CT).

The first scan was done at the resolution of $25 \mu\text{m}$ to understand the internal structure of coal. This scan was run at an X-ray beam energy of 80 kV and a power of 10 W. The distance between the specimen and X-ray source was 57.024 mm while there was 97.76 mm between the specimen and detector. An optical magnification of 0.4X was used to achieve high resolution. This gave a $25\text{-}\mu\text{m}$ pixel size and exposure time was set to 1.2 s in order to get intensity values for the best signal-to-noise ratio for each projection (radiograph). The next scan was done to achieve the resolution of $10 \mu\text{m}$ to focus on the most vitrinite half of the sample. The scan parameters for all samples are summarised in the Table 2. Having analysed 25- and $10\text{-}\mu\text{m}$ slides, the areas of interest were chosen, and four $2.5\text{-}\mu\text{m}$ slides were chosen with the most representative volume for porosity analysis and flow simulation.

Scanning electron microscopy technique was also exploited during the research but only of the upper surface of each sample at this stage. These SEM images were initially used for visual analysis of the width, integrity and mineralisation of the fractures to understand which parts of the sample should be targeted for scanning. Later, the samples were cut, and a few thin sections were prepared for further SEM analysis. Because the thin sections were extracted from different parts of the samples (not only from the surface) there will be an opportunity to calibrate micro-CT images with SEM data. The SEM images were obtained with magnification 22, 27 or 29, 100, 150, 250, 300 and 350 depending on the samples and the size of the features to be evaluated.

Table 1
Coal sample characteristics.

Sample ID	Sample (%)			Organic matter (%)			Vitrinite Reflectance ^o _{ran} (%)
	Organic matter	Pyrite	Others	Vitrinite	Inertinite	Liptinite	
PL3#-2	79.87	0.17	19.97	77.52	22.48	0.00	1.68



Fig. 2. Coal core sample polished and carbon-coated for SEM analysis.

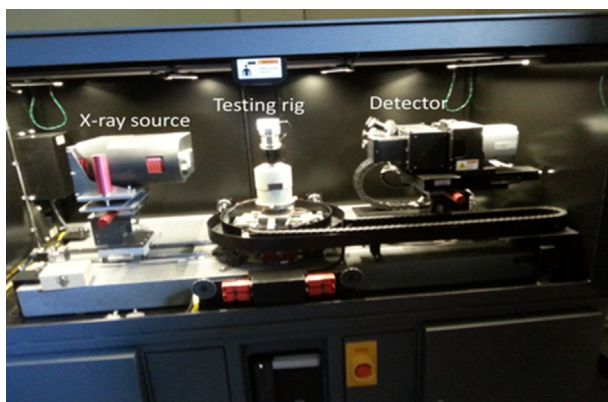


Fig. 3. ZEISS XRadia 410 Versa microscope [16].

4. Results

4.1. Grid independence test

Prior to calculating permeability of coal samples a grid independence test was carried out to validate the simulation method, and to find the best resolution for a sufficiently accurate numerical simulation. The test compared measured flow through a single fracture with constant width (defined by the average fracture width in the studied sample determined from 2.5- μ m scanned and 2.5- μ m subvoxelled images) to the analytical solution. The fracture width was 25 μ m, and the simulations were run for the following resolutions of the numerical

Table 2
Micro-CT scanning parameters.

Sample	Resolution, micron	Voltage, kV	Power, W	Distance to source, mm	Distance to detector, mm	Optical magnification	Exposure time, s
PL3#-2	25	80	10	57.0	97.8	0.4	1.2
PL3#-2	10	80	10	60.0	326.2	0.4	10
PL3#-2	2.5	120	10	65.0	110.0	4	15
PL3#-2	2.5	120	10	65.0	110.0	4	15
PL3#-2	2.5	120	10	65.0	110.0	4	15
PL3#-2	2.5	120	10	65.0	110.0	4	16

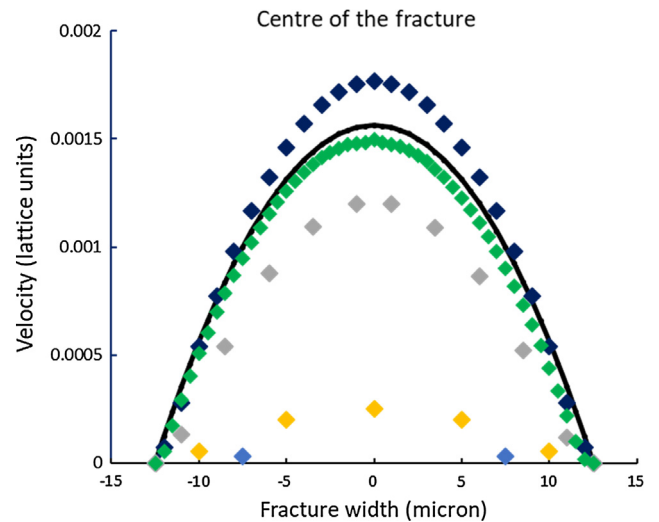


Fig. 4. Velocity profile across the fracture width: analytical solution (continuous black line) and numerical solution for different grid resolution (coloured symbols): blue – 2 cells per fracture width; yellow – 5 cells per fracture width; grey – 10 cells per fracture width; dark blue – 25 cells per fracture width; green – 50 cells per fracture width. (For interpretation of the references to colour in this figure legend, the reader is referred to the web version of this article.)

grid: 2, 5, 10, 25 and 50 cells per fracture width (i.e. 12.5, 5, 2.5, 1 and 0.5 μ m cell size, respectively). The comparison of the velocity profiles across the fracture with analytical solution is shown in Fig. 4. It was observed that for resolutions coarser than 10 cells per fracture width, there was a big discrepancy between analytical and numerical solutions. At the same time, the most accurate resolution was 50 cells per fracture width, as expected (Fig. 4). Resolutions 25 and 10 cells per fracture width show 15% and 18% discrepancy respectively, which was considered sufficiently accurate for the purpose of the study.

4.2. Subvoxel processing and segmentation

After micro-CT scans were obtained, images were processed and analysed versus SEM data, and it was found that the resolution of cleats is quite poor due to the partial volume effect, and the width of the cleats is overestimated for 25-, 10- and 5- μ m scans compared to the width obtained from SEM images (25 μ m determined from SEM and 100 μ m determined from 10- μ m micro-CT scans). On the other hand, the discrepancy between the widths of the cleats obtained from SEM and 2.5- μ m micro-CT scans is about 1–2 μ m. After couple unsuccessful attempts

to improve the resolution of cleats by application of different segmentation methods, the subvoxel processing algorithm was written and implemented in Matlab to overcome the partial volume effect. After analysis of SEM data and performing the grid dependence tests, we concluded that 2.5- μm resolution appears to be the best solution for the studied samples. The problem of scanning samples at 2.5- μm resolution is that the volume of investigation in case of this resolution is reduced to 2.5 mm*2.5 mm*2.5 mm which was not sufficiently large to be representative. Collecting series of separate volumes at 2.5- μm could have been a solution but it was difficult due to the scanning time and expenses. Thus, it was decided to take 10- μm images and improve the resolution of these images by subvoxel processing.

The idea to use subvoxel processing was taken from medicine [13] and is supposed to be applicable to volumes of interest containing materials or phases with two discrete signal intensities (coal matrix and cleats in the case of current research). The principal strategy consists of subdividing voxels and assigning voxel intensities to each subvoxel on the basis of local neighbourhood criteria.

However, the approach to subvoxel processing was adapted and the algorithm was written to be applicable for coal samples gray-scale images. Thus, the starting point of the algorithm for trabecular bones images was the partitioning of each voxel into eight subvoxels by strictly enforcing conservation of bone mass [13]. In order to ensure bone mass conservation, Hwang and Wehrli [12] generated bone volume fraction to determine the spatial distribution of trabecular bone. In the current research, the subvoxel processing was performed directly on the gray-scale images (where each voxel has a value from 0 to 255) and the restrictions to the algorithm were as follows: 1) the average sum of eight subvoxels values should be equal to the value of the original voxel, and 2) each subvoxel value could not exceed 255. Also, for trabecular bones images, each neighbouring pixel had the same contribution but if the resulting subvoxel was next to the voxels with zero BVF, this subvoxel was zeroed. With the current research, the following scheme was used: each voxel was partitioned into eight voxels (1, 2, 3, ... 8 in Fig. 5) and the resulting subvoxels were assigned the gray-scale intensity values based on the intensity values of neighbouring voxels, considering the proximity of each neighbour. Each subvoxel has 7 neighbours (for instance green, yellow and red voxels shown in Fig. 5 are the neighbours of the subvoxel 1): with 3 of them (green in Fig. 5) it has face-face connection, with 3 of them (yellow in Fig. 5) – edge-edge connection and with 1 of them (red in Fig. 5) – point-point connection. The weight of each neighbouring voxel is calculated based on the proximity to the subvoxel of interest: the weight of neighbouring voxels

with face-face connection is 25%, with edge-edge connection – 8% and with point-point connection – 1%. Subvoxel processing is an empirical algorithm rather than one derived from mathematical theory [13], so the optimal weighed contribution of each neighbouring voxel was determined by trying different configurations and comparing the subvoxelled images to the images scanned with higher resolution.

For the purpose of this research, the same volume of coal sample was scanned with different resolutions – 10-, 5- and 2.5- μm . Then, subvoxel processing was performed on 10- μm images a couple of times with different weighed contribution of neighbouring pixels (starting from equal weight of all neighbours and continuing towards an increase of contribution of face-face neighbours) and after each iteration, the results were compared to the scanned 5- μm images, and when the optimal result was achieved, subvoxel processing was repeated on subvoxelled images to achieve 2.5-resolution. Then, the resulting 2.5-subvoxelled images were compared to scanned 2.5- μm images for quality control. Images were compared in the following manner: the same features (similar intervals of cleats) were chosen on 5- and 2.5- μm scanned image and the width of cleats was determined by comparison with the one determined from SEM images. This calibrated width was then compared to the width of the same features obtained from 5- and 2.5- μm subvoxelled images. The results of subvoxel processing was accepted as optimal when the discrepancy between the width of analysed cleats was about 1–2 μm (less than 10% of the width). As a result of application of this method, the resolution of cleats was improved (Fig. 6) but the volume of investigation of new 2.5- μm subvoxelled images is 64 times bigger than that of 2.5- μm scanned images.

The next step of micro-CT scans analysis was image segmentation. Based on the experience of previous researchers, the [30] watershed method was chosen for image segmentation. This approach was successfully applied by Ramandi et al. for Australian coal samples, but used a combination of dry and wet coal images for better contrast between fractures and coal matrix. In the course of the current research coal was not saturated with any contrast fluid, and as a result of this, some unwanted noise appeared on segmented images which had to be removed by different filters. The most effective filter for the studies samples was median filter (Fig. 7).

4.3. Permeability simulation using LBM

Permeability of coal samples was determined from numerical simulations of steady state single-phase flow through the samples. Simulations were performed using Palabos, which is an open-source

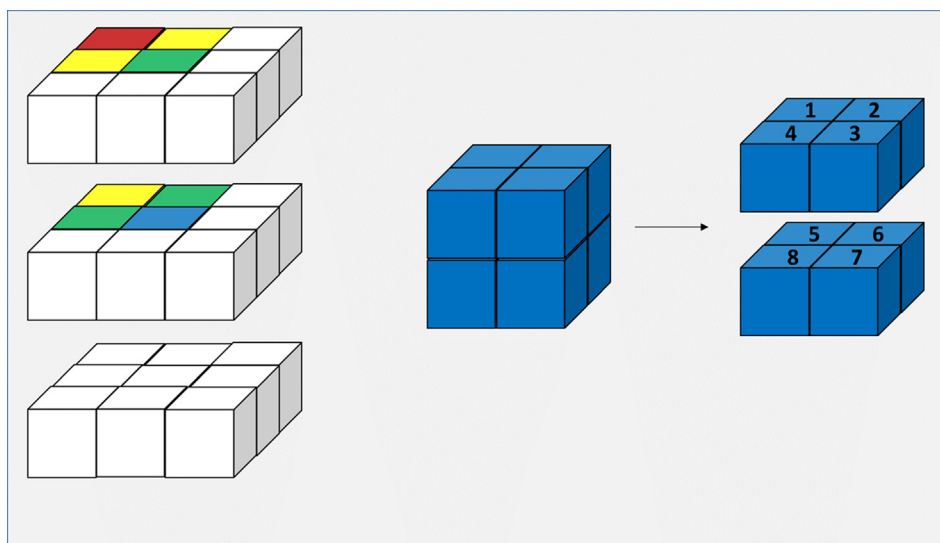


Fig. 5. Subvoxel partitioning scheme in 3D.

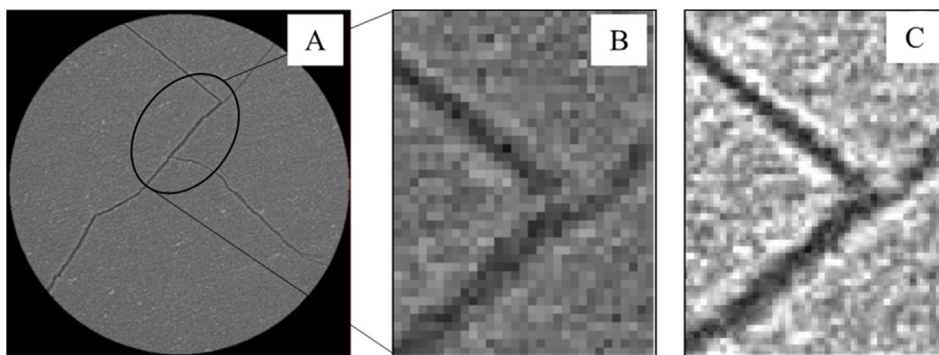


Fig. 6. An example of subvoxel processing results: A) 2.5-μm scanned image; B) 10-μm image before processing; C) 10-μm image after processing to 2.5-μm subvoxelled image.

computational fluid dynamics (CFD) solver based on the Lattice Boltzmann method. The Lattice Boltzmann method (LBM) is one of a number of particle-based CFD methods, where particles representing packets of fluid are tracked through the computational domain [3].

Permeability simulation was performed on three different sets of images: 10-μm scanned, 2.5-μm scanned and 2.5-μm subvoxelled (Fig. 8) to compare the results and estimate the sensitivity of permeability simulation to scanning resolution. For the simulation the following parameters were used: the D3Q19 lattice, bounce-back boundary conditions at the solid boundaries (walls), and a fixed pressure difference between the inlet and the outlet. A simulation starts with fluid having zero velocity, and with a constant pressure gradient in the x-direction (i.e. the principal flow direction). The permeability was computed by applying Darcy’s law to the simulated velocity data,

$$k = U\mu \frac{dx}{dp} \tag{1}$$

here U is average velocity in x-direction in the cleat, μ is the fluid viscosity and $\frac{dp}{dx}$ is the pressure gradient along the principal flow direction (i.e. between the inlet and outlet).

Since reconstruction of 3D geometry can produce slightly different results depending on the value of threshold applied in the segmentation process, for each set of images listed above, permeability simulation was performed several times. Table 3 summarises simulated permeability results according to the different thresholds used in segmentation process: in the course of each image set segmentation, three different points on each intensity histogram were chosen for watershed segmentation, and the resulted images were used for simulation. To sum all, the following results were obtained: permeability was determined in the range 75–125 mD for 2.5-μm subvoxelled images, in the range 125–205 mD for 2.5-μm scanned images, in the range

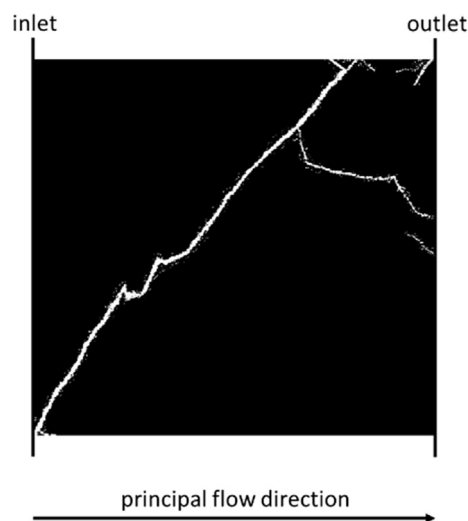


Fig. 8. An example of flow domain (2.5-μm scanned set) – the size of the sides is 2.5*2.5 mm.

Table 3
Simulated permeability results depending on segmentation thresholds.

Threshold point on histogram	Image set		
	2.5 scanned	2.5 subvoxelled	10 scanned
25%	125 mD	75 mD	2400 mD
50%	152 mD	88 mD	2670 mD
75%	205 mD	125 mD	3000 mD

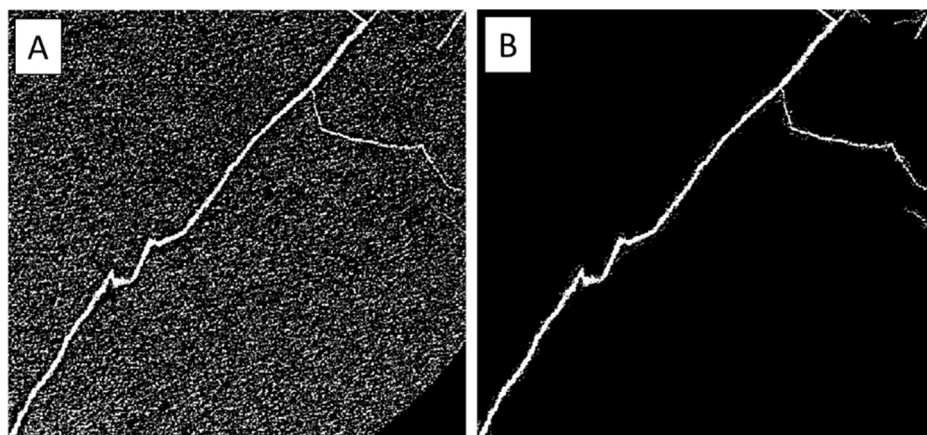


Fig. 7. The results of watershed- method segmentation in 2D and 3D – black is coal matrix, light colour – cleat: A) before noise removal; B) after noise removal.

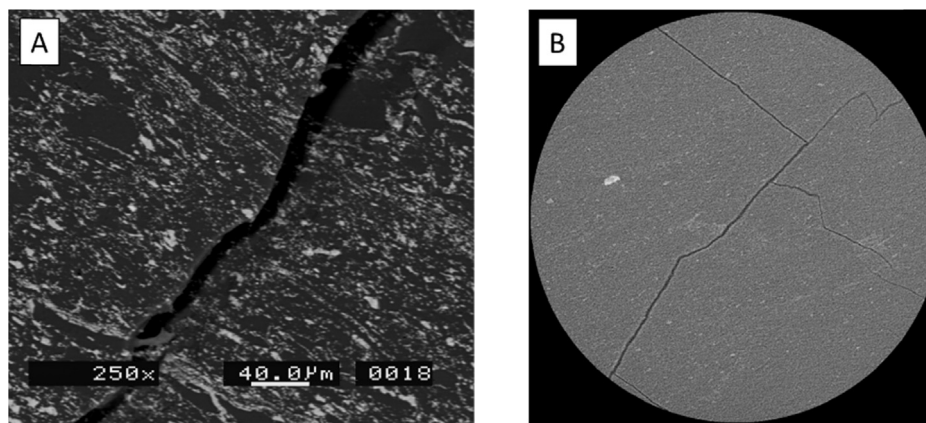


Fig. 9. SEM image (A) and micro-CT image (B) demonstrate that the fracture width is quite constant.

2400–3000 mD for 10- μm scanned images.

For the purpose of analytical solution, the fractures are assumed to have constant aperture d , to be parallel to the principal flow direction and to be at equal distances s , such that porosity of this system ϕ , is equal to the ratio d/s . Based on the analytical solution for Poiseuille flow between parallel plates the permeability of such system is:

$$k = \frac{\phi d^2}{12} \quad (2)$$

Previous researchers (e.g. [28]) claimed that fracture aperture should be measured as an average over a certain length. Analysis of SEM and micro-CT images of the samples used in this research showed that coal fractures of studied samples are quite constant and consistent in width (see Fig. 9), so it was decided to use average fracture aperture measured perpendicular to the main axis of fractures. Thus, analytical solution for the average fracture width (determined from 2.5- μm scanned and 2.5- μm subvoxelled images) gave the value of 82.5mD which is comparable with numerical simulation results.

5. Discussion, conclusion and future challenges

The research described in this paper focuses on implementation of micro-CT and SEM technologies for analysis of coal including improvement of image resolution, and the sample from Southern Qinshui Basin (China) was exploited for the research. It was observed that this coal was characterised by irregular cleat system which contained mainly thin fractures. This had two consequences: 1) poor resolution of those fractures due to the partial volume effect at lower resolutions (10- and 25- μm); 2) at higher resolution the scanned volume was too small to be representative of cleat system of those samples. Taking into account these two considerations, it was decided to use subvoxel processing algorithm to increase the resolution of 10- μm images to 2.5- μm but keeping volume of investigation of 10- μm images. This method was proven on 10- μm images but also later tested on different images with resolution from 25 to 2 μm . The idea for this approach was taken from medicine, but the approach was adapted to the area of the research and the algorithm was written based on the studied coal samples. The method was proved to overcome the partial volume effect, as long as cleat width is larger than the pixel size of a scan. It was also observed that there is no value in subvoxel processing below 2- μm resolution as it doesn't improve much the resolution of cleats. The establishing of subvoxel algorithm was utterly important for the current research as this algorithm allowed the authors to analyse coal thin features but significantly reduced the scanning time due to bigger volume of investigation of each scan.

The problem of optimal resolution required for permeability simulation, which provides a good balance between accuracy and efficiency, was also investigated in the course of this research. It was found that

the resolution that provides the most accurate permeability simulation (1.5% discrepancy with analytical solution) is 50 cells per fracture, which equates to 0.5- μm resolution. The minimal resolution for reasonably accurate simulation is 10 cells per fracture or 2.5 μm (18% discrepancy with analytical solution). In the future, 2.5- μm resolution will be used as a standard to work with these samples.

In the course of this research, the permeability simulation was also performed on different images (with different resolution) and compared with analytical solution for Poiseuille flow in a single crack. Permeability simulation was performed for two reasons: 1) it was required for validation of the results of image subvoxelling and segmentation, and 2) the results obtained on mm-scale will further be used to upscale permeability to cm-scale. Numerical simulation demonstrated that the permeability simulated on 2.5- μm scanned images is in accordance with the permeability obtained for 2.5- μm subvoxelled images (125–205 mD and 75–125 mD correspondingly), while 10- μm scanned images gave the permeability in the range 2400–3000 mD. Considering that the analytical solution for an average fracture width gives permeability 82.5mD, it was concluded that simulation for 10- μm scans greatly overestimated permeability. The latter supports the observation that the width of cleats determined from 10- μm scanned images was also overestimated compared to the one obtained from SEM data. However, the permeability obtained from the simulation is greater than the expected from the analysis of coal samples from the studied coal basin. This was probably due to the scale effect, i.e. to the fact that only a limited volume of coal was used for simulation. Moreover, this volume contained a couple of fractures with considerable width, which increased the porosity of the sample up to 4%. Analysis of the whole sample shows that the cleat porosity of the sample was lower (about 1.8%). Laboratory measurements of permeability of studied coal samples are in progress at the moment but available data from the studied basin show that coal permeability is in the range 0.01–0.37 mD [22].

The research described in this paper was performed at mm-scale and the problem of upscaling permeability data to get permeability for the whole sample, as well as the validation of upscaling, is not discussed in this paper. One possible way of addressing this challenge is to identify the key features from rock images, e.g., self-similar behaviour [38], which control the flow behaviour at different scale and then apply the feature based approach [32,33] to estimate the permeability at different scale. Finally, it must be noted that the research described in this paper considered only cleat porosity and permeability. Pore matrix porosity will be investigated at the next stage of the research.

Acknowledgment

This paper utilised opportunistic coal samples and characterisation data as a part of a study into multiphase flow in coal for Southern Qinshui coal basin. The measurement of this work was supported by the

Royal Society through the International Cost Share Project, and Alexandra would like to thank Ministry of Education of Russia to support her PhD work at University of Aberdeen. The University of Aberdeen School of Engineering and School of Geosciences are thanked for their support. The authors also thank John Still from The University of Aberdeen School of Geosciences for his support regarding SEM data analysis and Amir Golparvar from The University of Aberdeen School of Engineering for his help with Matlab.

References

- [1] Arns CH, Bauget F, Limaye A, Sakellariou A, Senden TJ, Sheppard AP, et al. Pore-scale characterization of carbonates using X-ray microtomography. *SPE J* 2005;10(4):475–84.
- [2] Arns JY, Sheppard AP, Arns CH, Knackstedt MA, Yelkhovsky A, Pinczewski WV. Pore-level validation of representative pore networks obtained from micro-CT images. Proceedings of the annual symposium of the society of core analysis, SCA 2007-A26. 2007. Calgary, Canada.
- [3] Blunt MJ, Bijeljic B, Dong H, Gharbi O, Iglauer S, Mostaghimi P, et al. Pore-scale imaging and modelling. *Adv Water Resour* 2013;51:197–216.
- [4] Cai Y, Liu D, Yao Y, Li J, Qiu Y. Geological controls on prediction of coalbed methane of No. 3 coal seam in Southern Qinshui Basin, North China. *Int J Coal Geol* 2011;88:101–12.
- [5] Carlson WD, Rowe T, Ketcham RA, Colbert MW. Applications of high resolution X-ray computed tomography in petrology, meteoritics and paleontology. In: Mees F, Swennen R, Van Geet M, Jacobs P, editors. Applications of X-ray Computed Tomography in the Geosciences: Geological Society. London: Special Publication; 2003. p. 7–22.
- [6] Clarkson CR, Bustin RM. Variation in micropore capacity and size distribution with composition in bituminous coal of the Western Canadian Sedimentary Basin: implications for coalbed methane potential. *Fuel* 1996;75:1483–98.
- [7] Ersoy O, Şen E, Aydar E, Tatar İ, Çelik HH. Surface area and volume measurements of volcanic ash particles using micro-computed tomography (micro-CT): a comparison with scanning electron microscope (SEM) stereoscopic imaging and geometric considerations. *J Volcanol Geoth Res* 2010;196:281–6.
- [8] Flannery BP, Deckman HW, Roberge WG, D'Amico KL. Three-dimensional X-ray microtomography. *Science* 1987;237:1439–44.
- [9] Giffin S, Littke R, Klaver J, Urai JL. Application of BIB-SEM technology to characterise macropore morphology in coal. *Int J Coal Geol* 2013;114:85–95.
- [10] Golab A, Knackstedt MA, Averdunk H, Senden T, Butcher AR, Jaime P. 3D porosity and mineralogy characterization in tight gas sandstones. *Lead Edge* 2010;936–942(December).
- [11] Golab A, Ward CR, Permana A, Lennox P, Botha P. High-resolution three-dimensional imaging of coal using microfocus X-ray computed tomography, with special reference to modes of mineral occurrence. *Int J Coal Geol* 2013;113:97–118.
- [12] Hwang SN, Wehrli FW. Estimating voxel volume fractions of trabecular bone on the basis of magnetic resonance images acquired in vivo. *Int J Imaging Syst Technol* 1999;10:186–98.
- [13] Hwang SN, Wehrli FW. Subvoxel processing: a method for reducing partial volume blurring with application to in vivo MR images of trabecular bone. *Magn Reson Med* 2002;47(5):948–57.
- [14] Jing Y, Armstrong RT, Ramandi HL, Mostaghimi P. Coal cleat reconstruction using micro-computed tomography imaging. *Fuel* 2016;181:286–99.
- [15] Karachan CO, Okandan E. Adsorption and gas transport in coal microstructure: investigation and evaluation by quantitative X-ray CT imaging. *Fuel* 2001;80:509–20.
- [16] Kartal M, Dugdale LH, Harrigan JJ, Siddiq M, Pokrajac D, Mulvihill DM. Three-dimensional in situ observations of compressive damage mechanisms in syntactic foam using X-ray microcomputed tomography. *J Mater Sci* 2017;52:10186–97.
- [17] Ketcham RA, Carlson WD. Acquisition, optimization and interpretation of X-ray computed tomographic imagery: applications to the geosciences. *Comput Geosci* 2001;27:381–400.
- [18] Knackstedt M, Arns C, Senden TJ, Gross K. Structure and properties of clinical coralline implants measured via 3D imaging and analysis. *Biomaterials* 2006;27(13):2776–86.
- [19] Knackstedt M, Jaime P, Butcher AR, Botha PWSK, Middleton J, Sok R. Integrating reservoir characterization: 3D dynamic, petrophysical and geological description of reservoir facies. Proceedings of the SPE Asia Pacific oil and gas conference and exhibition. Brisbane, Queensland, Australia: SPE; 2010. p. 133981.
- [20] Knackstedt M, Carnerup A, Golab A, Sok R, Young B, Riepe L. Petrophysical characterization of unconventional reservoir core at multiple scales. *Soc Petrophys Well-Log Anal* 2013;54(03).
- [21] Lemmens HJ, Butcher AR, Botha PWSK. FIB/SEM and automated mineralogy for core and cuttings analysis. Proceedings of the SPE Russian oil and gas conference and exhibition. Moscow, Russia: SPE; 2010. p. 136327.
- [22] Li C, Liu D, Cai Y, Yao Y. Fracture permeability evaluation of a coal reservoir using geophysical logging: a case study in the Zhengzhuang area, southern Qinshui Basin. *Energy Explor Exploit* 2016;34(3):378–99.
- [23] Long J, Young G, Holland T, Senden T, Fitzgerald E. An exceptional Devonian fish from Australia sheds light on tetrapod origins. *Nature* 2006;444:199–202.
- [24] Mazumder S, Wolf K-HAA, Elewaut K, Ephraim R. Application of X-ray computed tomography for analyzing cleat spacing and cleat aperture in coal samples. *Int J Coal Geol* 2006;68:205–22.
- [25] Moore TA. Coalbed methane: a review. *Int J Coal Geol* 2012;101:36–81.
- [26] Mostaghimi P, Armstrong RT, Gerami A, et al. Micro-CT imaging and microfluidics for understanding flow in coal seam reservoirs. Paper presented at the International Symposium of the Society of Core Analysts. 2015. Newfoundland, Canada, 16–21 August.
- [27] Novelline R. Squire's fundamentals of radiology. Cambridge, Massachusetts: Harvard University Press; 1997. p. 638.
- [28] Oron AP, Berkowitz B. Flow in rock fractures: The local cubic law assumption re-examined. *Wat Resour Res* 1998;34(11):2811–25.
- [29] Puri R, Evanoff J, Brugler M. Measurement of coal cleat porosity and relative permeability characteristics. Paper presented at the SPE Gas Technology Symposium. 1991. Houston, Texas.
- [30] Ramandi HL, Mostaghimi P, Armstrong RT, Pinczewski WV. Porosity and permeability characterization of coal: a micro-computed tomography study. *Int J Coal Geol* 2016;154–155:57–68.
- [31] Roberts R, Senden TJ, Knackstedt MA, Lyne MB. Spreading of aqueous liquids in unsized papers is by film flow. *J Pulp Pap Sci* 2003;29:123–30.
- [32] Singh H, Cai J. A feature-based stochastic permeability of shale: part 1—validation and two-phase permeability in a utica shale sample. *Transp Porous Media* 2018;126(3):527–60.
- [33] Singh H, Cai J. A feature-based stochastic permeability of shale: part 2—predicting field-scale permeability. *Transp Porous Media* 2018;126(3):561–78.
- [34] Simons FJ, Verhelst F, Swennen R. Quantitative characterization of coal by means of microfocus X-ray computed tomography (CMT) and colour image analysis (CIA). *Int J Coal Geol* 1997;34:69–88.
- [35] Van Geet M, Swennen R. Quantitative 3D-fracture analysis by means of microfocus X-ray computer tomography (micro-CT): an example from coal. *Geophys Res Lett* 2001;28(17):3333–6.
- [36] Verhelst F, David P, Fermont W, Jegers L, Vervoort A. Correlation of 3D-computerised tomographic scans and 2D-colour image analysis of Westphalian coal by means of multivariate statistics. *Int J Coal Geol* 1996;29:1–21.
- [37] Wang H, Yao Y, Liu D, Pan Z, Yang Y, Cai Y. Fault-sealing capability and its impact on coalbed methane distribution in the Zhengzhuang field, southern Qinshui Basin, North China. *J Natural Gas Sci Eng* 2016;28:613–25.
- [38] Wu H, Zhou Y, Yao Y, Wu K. Imaged based fractal characterization of micro-fracture structure in coal. *Fuel* 2019;239:53–62.
- [39] Wu K, Van Dijke MJJ, Couples GD, Sorbie KS, Ma J. 3D stochastic modelling of heterogeneous porous media—applications to reservoir rocks. *Transport Porous Media* 2006;65(3):443–67.
- [40] Yao Y, Liu D, Che Y, Tang D, Tang S, Huang W. Non-destructive characterization of coal samples from China using microfocus X-ray computed tomography. *Int J Coal Geol* 2009;80:113–23.
- [41] Zezabe R, Jones A, Knackstedt M, Seeman E. Femoral neck shape and the spatial distribution of its mineral mass varies with its size: clinical and biomechanical implications. *Bone* 2005;37(2):243–52.